J Mater Sci: Mater Electron (2014) 25:444–453
DOI 10.1007/s10854-013-1608-1

The effect of Nd_2O_3 addition on superconducting and structural properties and activation energy calculation of *Bi-2212* superconducting system

O. Ozturk · E. Asikuzun · M. Coskunyurek · N. Soylu · A. Hancerliogullari · A. Varilci · C. Terzioglu

Received: 28 June 2013 / Accepted: 8 November 2013 / Published online: 19 November 2013

Abstract The effect of Nd_2O_3 addition on the microstructural and the superconducting properties of *Bi-2212* superconductor ceramics, prepared by solid state reaction method, was analyzed by performing X-ray diffraction (*XRD*), scanning electronic microscope (*SEM*), energy dispersive spectroscopy (*EDS*) and dc Resistivity (ρ-*T*) measurements. The magnetoresistivity of the samples was measured for different values of the applied magnetic field strengths (0–7 T). Also, the activation energies were calculated using the Arrhenius equation. According to these results, the T_c^{offset} value of the undoped sample was decreased from 79 to 42 K with the growth of magnetic field. In the same way, the activation energy (U_o) values were significantly diminished by the increasing of magnetic field. A similar situation was observed in other doped samples. Activation energy for 0.05 % Nd_2O_3 doped sample under 7 T magnetic field was 550 J/mol the least. In addition, lattice parameter *c*, calculated by analysis of *XRD* data, was decreased with doping while lattice parameter *a* was increased. *SEM* analysis shows that particles were shrinking with the addition. When compared with other elements for *EDS* analyses, it was analyzed an important decrease in the percentage of *Sr* with the increasing of *Nd* contribution.

O. Ozturk (✉) · E. Asikuzun · M. Coskunyurek · A. Hancerliogullari
Department of Physics, Faculty of Arts and Science, Kastamonu University, 37100 Kastamonu, Turkey
e-mail: oozturk@kastamonu.edu.tr

N. Soylu · A. Varilci · C. Terzioglu
Department of Physics, Faculty of Arts and Science, Abant Izzet Baysal University, 14280 Bolu, Turkey

1 Introduction

The discovery of high temperature superconductor materials has generated great interest of the scientific community for many reasons [1]. Since high-T_c cuprate superconductors are chemically unstable and highly reactive, most materials including the noble metals and oxides react with these superconductors when they come into contact. Scientists have strived to improve their superconducting, physical, mechanical, structural, and flux pinning properties to make them suitable for high temperature and magnetic field applications [2–4]. Bi–Sr–Ca–Cu–O system is an important member of the high-T_c superconductor families with an orthorhombic structure and it has been found at least in three phases with atomic ratios in the order of Bi, Sr, Ca, Cu, namely (2201), (2212) and (2223) with zero resistivity transition temperatures of 20, 85 and 110 K, respectively [5, 6]. Bi-based superconductors have attracted the attention of many researchers for potential technological and industrial applications due to the their remarkable smaller power losses, high current, and magnetic field carrying capacity, electronic and optical properties [7–13].

Superconducting materials are prone to technological applications and are materials in progress to date. The common idea of many scientists, studying in the field, is that the technological application of superconductivity may be unexpectedly begin. The possible fields of application of the subject can be exemplified by the underground electric power transmission systems, slightly magnetic transport system, waste fluid treatment system, transformers, magnetic field sensors, and infrared sensors. Superconductors are used frequently especially in the focusing beam at accelerator mass systems at CERN in recent years [14], in the conception of the new generation reactor system in

fusion technology, and in confining the plasma in a magnetic field using triodal systems. For this reason, the characterization studies of every superconducting material should be performed with the most versatility and concise to ensure and facilitate the usage in the above mentioned field.

The focus of this study is to determine the activation energies of fabricated materials that are one of important characterizations for materials. The excitation energy is certainly needed to start all endothermic and exothermic reactions. Because it is required for the particles collide with a certain intensity and frequency in order to start reacting. Energy is needed for all reactions to begin. This is called the activation energy. Activation energy identified in both collision theory and transition state theory that is the required energy for substances in reaction to make activated complex. Activation energy makes them more active rising the internal energy of the reactants.

It is unlikely a reaction thermodynamically to happen without the activation energy. This energy is spent on such matters as the weakening or rupture of the bonds, or the approximation of the molecules to each other defeating the thrust forces. The activation energy is provided for the kinetic energy of the colliding particles to make a reaction. The higher the activation energy is, more important to the dependence of reaction rate on temperature. The speed of reaction to small activation energy increases slightly with increasing temperature. But, the speed of reaction with high activation energy shows much commitment to temperature.

Various techniques and methods are used to calculate the activation energy. The activation energy of samples can be calculated based on the DTA analysis and resistivity measurements [15]. The DTA analysis has importance in the subject field of the crystallization kinetics on the glass and in the calculation of activation energy. Activation energies of the sample can be calculated with the Kissinger method developed by Kissinger and Augis Bennet method using DTA data. It is possible to calculate the activation energy using R–T measurements [16–19]. This study uses Arrhenius relation to calculate activation energy.

$$\rho = \rho_0 \exp(-U_0/k_B T) \quad (1)$$

Here U_0 is activation energy, ρ is resistivity in T temperature, ρ_0 is resistivity in the first temperature and k_B is the Boltzman constant.

In this study, the effect of Nd_2O_3 addition of superconducting and micro-structural properties of doped and undoped *Bi-2212* ceramics, produced by solid-state reaction method, has been investigated using X-ray diffraction (*XRD*), scanning electronic microscope (*SEM*), energy dispersive spectroscopy (*EDS*) and resistivity measurements with and without magnetic field. Some properties of the samples such as superconducting transition temperature and activation energy can be determined with resistivity measurements made under magnetic field. When the results are taken into considerations, it is seen that physical, structural, and superconducting properties of the samples have changed with *Nd* addition.

2 Experimental

In this study, Nd_2O_3 (Alfa Aesar Co., Ltd. 99.9 % purity) at the rate of $x = 0.001$, 0.005, 0.01, 0.05, 0.1 % has been doped to $Bi_2Sr_2CaCu_2O_x$ (Alfa Aesar Co., Ltd. 99.9 % purity) superconducting powder. Undoped sample was produced under the same conditions for comparison with doped samples. The powder mixture was compacted into tablets each under the pressure of 7 tons, 13 mm in diameter and 1–1.5 mm thick. Then, tablets were put in high temperature programmable tube furnace in room temperature and annealed for 72 h at 840 °C. The heating and cooling rates of the furnace were adjusted to be 5 °C/min.

The electrical resistivity versus temperature measurements were performed at various applied dc magnetic fields (0–7 T) at constant driving current of 5 mA. The magnetic fields generated from the superconducting coil magnet from *CRYO* Industries were applied normal to the direction of the driving current. Measurements were done by the standard four-point technique, both voltage and current contacts were made with silver paint in order to minimize the contact resistance. For these measurements, *Keithley 220* programmable current source, *Keithley 2182A* nanovoltmeter and He gas contact cryostat (closed-cycle) from *CRYO* Industries were used. Transition temperature for superconductivity was decided as T_c^{offset} the temperature in which resistance decreases and superconductivity begins. *XRD* analyses were performed by *Bruker D8 Advance* model diffractometer, using CuKα radiation (1.54 Å), in the range of $2\theta = 3$–60° at a scanning rate of 1°/min and step increment of 0.02° at room temperature in air atmosphere. The *XRD* curves obtained allow us to calculate the lattice constant parameters and volume fraction values. The average crystallite size is also determined from the Scherrer–Warren approach. As for the *SEM* investigations, the surface morphology, grain size distribution, connectivity between the superconducting grains and grain boundary weak-links in the Nd_2O_3 doped and undoped *Bi-2212* bulk superconductors were determined using a scanning electron microscope *JEOL 6390-LV*, operated at 20 kV, with a resolution power of 3 nm. And lastly *EDS* analysis was performed to determine the amount of ion changing with doping. In addition, the activation energy of all the samples was calculated by using resistivity

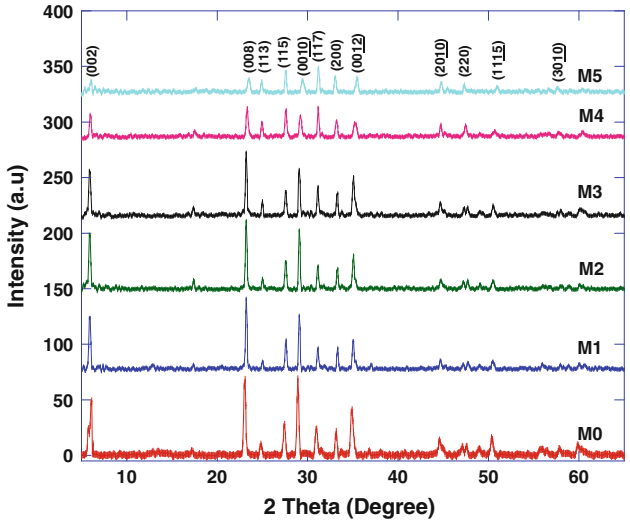

Fig. 1 *XRD* patterns for the all samples

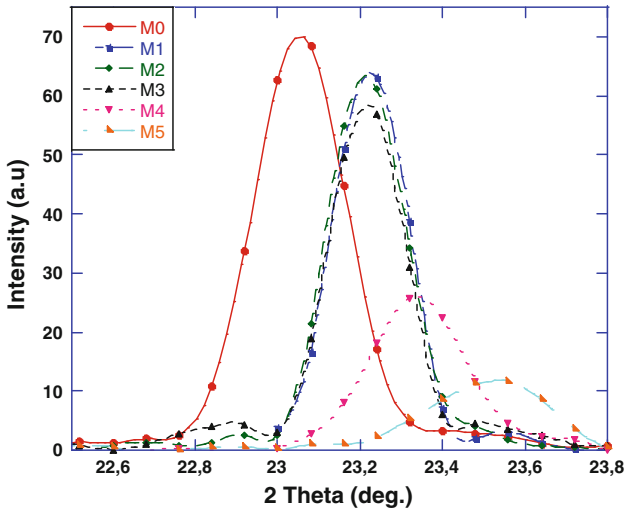

Fig. 2 *XRD* peaks for the (008) plane

Table 1 Lattice parameter, volume fraction and grain size values for the all samples

Samples	*c* (Å)	*a* (Å)	Volume fraction		Grain size (Å)
			Bi-2212 (%)–*Bi-2201* (%)		
M0	31.33	5.35	95	5	107.86
M1	30.49	5.37	96	4	97.29
M2	30.45	5.38	93	7	85.41
M3	30.43	5.39	91	9	61.85
M4	30.26	5.40	86	14	47.38
M5	30.06	5.41	78	22	34.33

measurements under magnetic field. Henceforth, undoped and Nd_2O_3 doped materials at rates of $x = 0.0$, 0.001, 0.005, 0.01, 0.05, 0.1 % will be referred in the order of *M0*, *M1*, *M2*, *M3*, *M4* and *M5*.

3 Results and discussion

3.1 *XRD* analyses

X-ray diffraction measurements of the *M0*, *M1*, *M2*, *M3*, *M4* and *M5* samples in the range of $3 < 2\theta < 60$ prepared with the solid state reaction with heat treated for 72 h at 840 °C were made with scan rate 0.5 °/min. The obtained *XRD* peaks are shown in Fig. 1. *a* and *c* lattice parameters belonging to structure are calculated for orthorhombic and the following results were obtained by using the method of the least squares method of the shown *XRD* peaks.

As shown in Table 1, the *c* parameters of the samples are decreased with the increasing of Nd_2O_3 contribution. The highest value belongs to undoped *M0* sample (31.33 Å). Change in lattice parameters can be summarized as follows. In high temperature superconductors, when the rare-earth dopants with $+3$ valance are replaced with *Sr* or *Ca* with $+2$ valance, 1 electron joined the structure causes an increase in oxygen content. The excess in the oxygen is taken by *Bi–O* binary planes which is oxygen poor. After all, the positive charge in *Bi–O* layers is reduced and the driving force between the positive charges is reduced. Attachments become more stringent. This behaviour reduces *Bi–O* layers and causes a decrease in the length of *c* axis [20–22].

Generally, when it is compared with *Sr* or *Ca*, a small ionic radius of the doped ion can also decrease *c* lattice parameter by increasing the oxygen amount (Ca^{+2} = 0.990 Å, Sr^{+2} = 1.130 Å, Nd^{+3} = 0.995 Å) in the system [13, 23]. In fact, *EDS* results of our study support that *Nd* may be mainly replaced by *Sr*.

A systematic increase is observed in parameters with the increase of Nd_2O_3 contribution. This is the expected situation happening with the emergence of *Nd* addition and extra electrons. The effective valence of *Cu* atoms with the addition is decreased, and this behaviour caused the growth of the length *Cu–O* bond and consequently increased *a* parameters [24, 25].

When looked at the volume ranges according to the change in the amount of the addition, it was found that low temperature phase (%V2212) is decreased with the addition and the very low temperature phase (%V2201) is increased with the addition (Table 1). This result proves that very low temperature phase (%V2201) is more dominant with the increasing addition.

Moreover, *XRD* peak of (008) plane has been illustrated in Fig. 2. With the increase of Nd_2O_3 doped, peaks

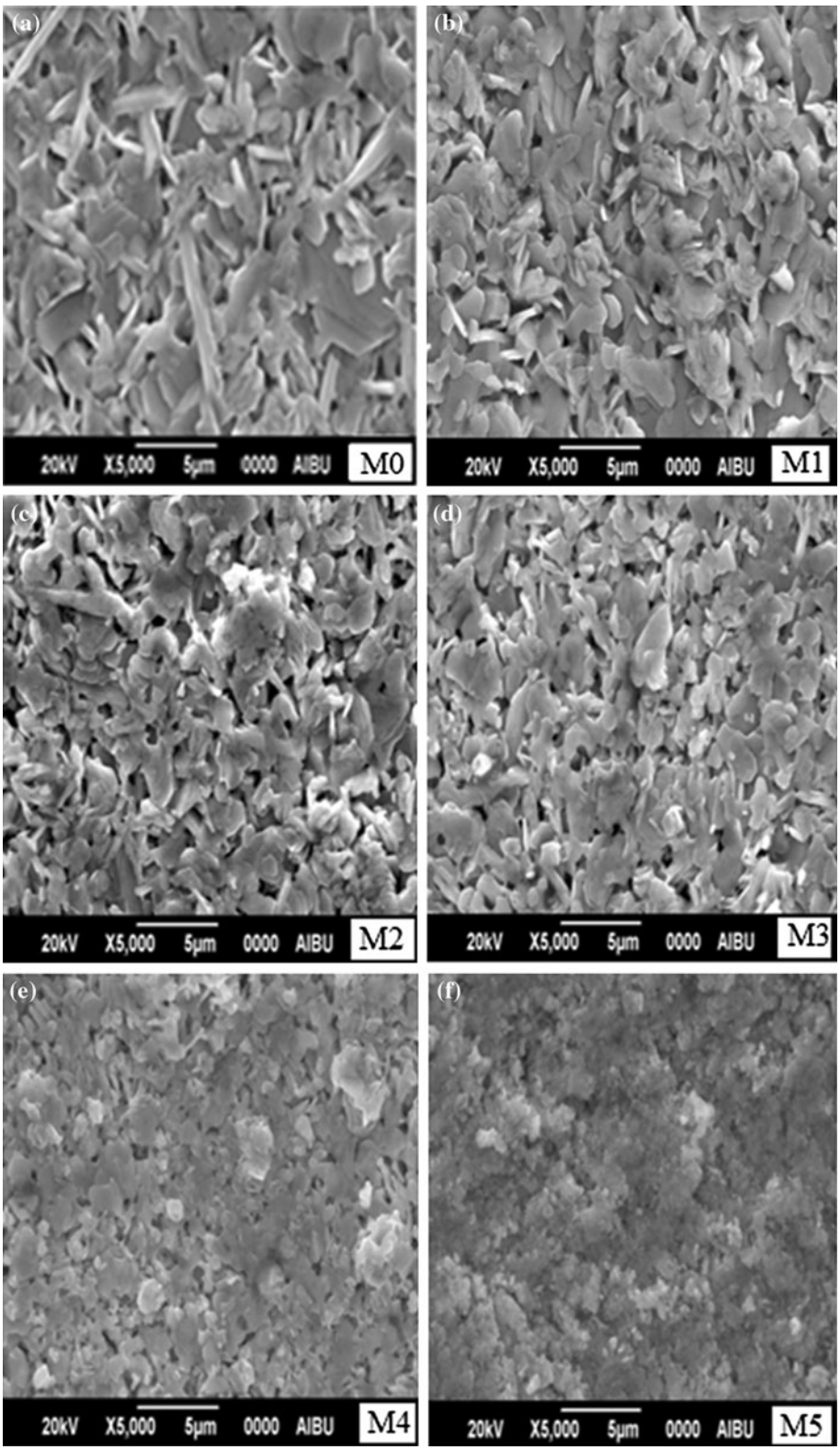

Fig. 3 *SEM* micrographs for the all samples

have shifted to greater angles. This shift is an indicator of the decrease in *c* axis with increasing *Nd* doping. In addition to this, as it is obviously seen in Fig. 2, the peak intensity has diminished with the growth of doped amount. The grain's getting smaller is the reason of this effect.

3.2 Grain size calculation by Scherrer–Warren approach

Grain size is one of the important parameters which is calculated using X-ray diffraction analyses. The average grain sizes of the samples are calculated with the Scherrer–Warren method [26, 27].

$$D = 0.94\lambda/B\cos\theta \quad (2)$$

$$B^2 = B_s^2 - B_m^2 \quad (3)$$

is given by equations above [28–30]. Here D is the grain size, λ is the wavelength of the X-ray, B_s is the full width which is half of the maximum peak intensity and this value (FWHM) is measured in radian. B_m is a constant value. θ is an angle belonging this peak. Grain size calculations are given in Table 1. When data according to different amounts of Nd_2O_3 addition are analyzed, it has been found that *M0* sample annealed at 840 °C for 72 h has biggest grain size, in other words, grain size decreased with addition. This event is also confirmed by *SEM* images.

3.3 *SEM* analyses

In order to determine the grain sizes, possible precipitation at the grain boundaries and the structure of surface morphology of the samples are analyzed by using scanning electron microscope. *SEM* images in 5,000 magnification of all the undoped and Nd_2O_3 doped *Bi-2212* samples are given in Fig. 3. When the images are analyzed, it is proved that the grains with Nd_2O_3 doping are decreased and there is a little melting. The results of the calculated grain sizes by using *XRD* peaks respectively are found as 107.86, 97.29, 85.41, 61.85, 47.38 and 64.86 Å. According to these results, calculations of grain size using *XRD* data support our *SEM* interpretations. Also, a flaky grain characteristic feature of *Bi-2212* phase is evident in all samples.

3.4 *EDS* analyses

Energy dispersive spectroscopy is a technique used for elemental analysis working in the 0–30 keV energy range. The elemental composition analyses are possible for almost all of the elements with this technique. The elemental composition analyses of the samples are analytically investigated by the *EDS* investigations. Similar to the *SEM* results, we give the element concentration of all samples in Fig. 4. Also ion amounts changing with the addition are given in Table 2. As it is clear in the table, while there is not a critical change in oxygen amount, when compared with other elements, there is a crucial decrease in the percentage of *Sr* with the increase of Nd_2O_3 addition. As a result, Nd^{+3} ions enter into the crystal structure by replacing mainly with Sr^{+2} ions [31].

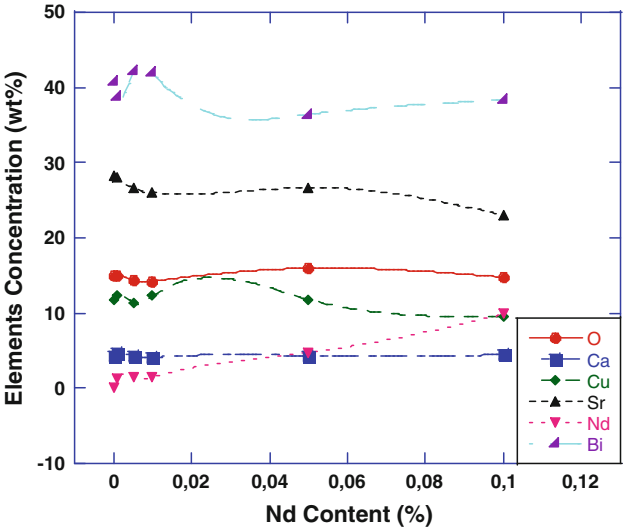

Fig. 4 Variation of elements concentration with *Nd* content

Table 2 Concentrations of the elements for the samples

Component	Concentration (wt%)					
	M0	*M1*	*M2*	*M3*	*M4*	*M5*
O	14.92	15.07	14.30	14.20	15.79	14.78
Ca	4.34	4.62	4.24	4.11	4.21	4.43
Nd	–	1.22	1.40	1.52	5.46	9.85
Cu	11.69	12.26	11.35	12.27	10.36	9.52
Sr	28.33	27.98	26.62	26.00	26.31	23.07
Bi	40.69	38.82	42.05	41.87	37.85	38.32

3.5 Carrier concentration calculation

The hole-carrier concentrations per *Cu* ion, p, are calculated by using the following relation [32–34].

$$T_C/T_C^{\max} = 1 - 82.6\,(p - 0.16)^2 \quad (4)$$

Here p, carrier concentration; T_c, the temperature at which the resistance is zero; T_c^{max} is 85 K, the superconducting transition temperature for *Bi-2212* superconductor [35]. As a result of calculations, the carrier concentrations changing when Nd^{+3} is doped, have been illustrated in Table 3. Upon the doping of Nd^{+3} to the system, a decrease occurs in the carrier concentration. The optimal value of the carrier concentration can be seen in the undoped sample. According to this change, the valence level of copper can be adjusted. Considering that Nd^{+3} ions mainly replaces with Sr^{+2} ions, it provides an extra electron to the system. This situation has caused a transition from low temperature (*Bi-2212* phase) to extra low temperature (*Bi-2201* phase). This phase transition has caused the decrease of T_c^{offset} values, as seen in ρ-T measurements.

Table 3 T_c^{offset}, ΔT_c, hole concentrations and room temperature resistivity values for the all samples

Samples	T_c^{offset} (K)							ΔT (T_c^{onset} − T_c^{onset}) (for 0 T)	Hole conc. (p)	Room temp. resistivity (Ω mm)
	0 T	0.5 T	1 T	2 T	3 T	5 T	7 T			
M0	79	52	52	47	45	43	42	5.9	0.105	0.100
M1	59	51	46	42	39	37	35	26	0.099	0.101
M2	59	49	45	40	39	36	34	26	0.099	0.146
M3	58	47	45	40	39	35	34	27	0.098	0.273
M4	50	28	26	24	24	23	20	35	0.089	0.404

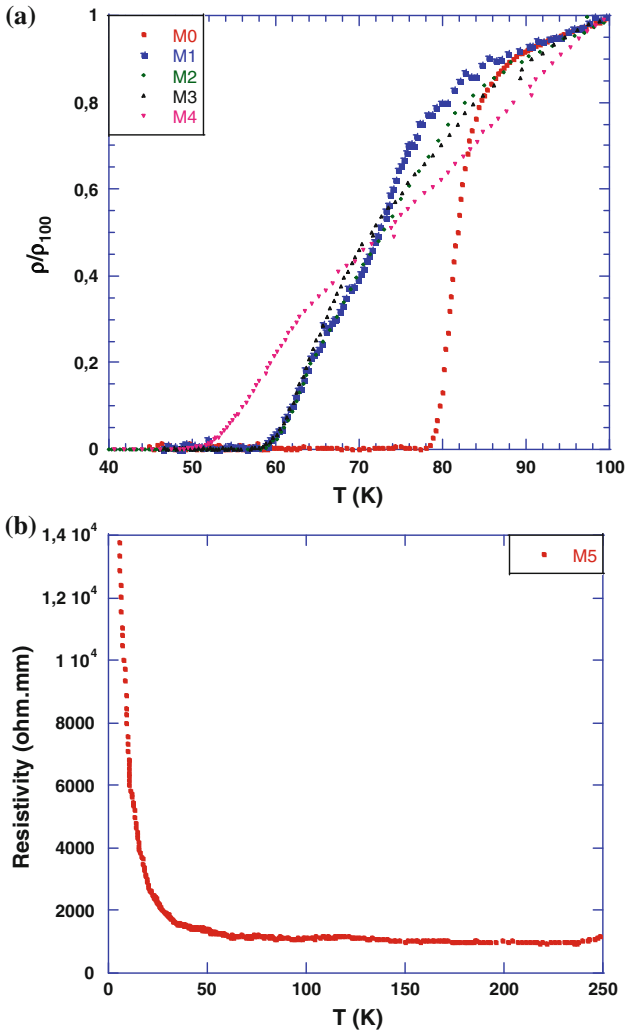

Fig. 5 Normalized resistivity as a function of temperature curves for the samples

3.6 Electrical resistivity measurements

The electrical resistivity measurement has been done to examine the effect of Nd_2O_3 addition on the superconducting properties of the samples. Figure 5a shows the variation of normalized resistivity of the samples (*M0*, *M1*, *M2*, *M3* and *M4*) with temperature. Figure 5b provides *M5* resistivity–temperature graph of samples. Metallic behavior over T_c value is observed on all samples except for *M5* sample. *M5* shows an insulating property with the addition. Grains are decreased and contact points are increased with the increasing Nd_2O_3 addition. Accordingly, the resistivity of room temperature increase as seen from Fig. 3. Critical temperatures, in which samples show zero resistance, for *M0*, *M1*, *M2*, *M3* and *M4* samples are 79, 59, 59, 58, and 50 K, respectively (Fig. 3). The decrease in the values of Nd_2O_3 addition and T_c^{offset} can be associated with the reduction *Bi-2201* phase. The value of ΔT_c increases with the addition. This value for undoped samples (*M0*) is 5.9 K while it is 35 K for *M4* sample. The increase in resistivity with the increase Nd_2O_3 addition can be caused by weak links between superconductor grains and the presence of impurity phase. Also, carrier concentration decreased with decreasing the addition (Table 3). Thus, the reduction in T_c can be caused by the reduction of charge carriers.

3.7 Magnetoresistivity measurements

The temperature dependence of the resistivity in an external magnetic field ranging from 0 to 7 T for the doped and the undoped *Bi-2212* samples, fabricated by the conventional solid-state reaction method, is measured in the temperature range 20–120 K. The temperature dependence of magnetoresistivity for all samples is shown in Fig. 6. As it is clearly seen from figure, T_c^{offset} value is decreased with the increase in magnetic field. There is no significant change in the value of T_c^{onset}.

The T_c^{onset} and T_c^{offset} values of the materials are related to the superconducting transition of the grains and volume fraction or properties of the intergranular components, respectively [36, 37]. Therefore the applied magnetic field affect mostly the pairs between the grains of superconducting materials. While the T_c^{onset} values of the sample did not change significantly, T_c^{offset} values decrease to important extent along with the applied magnetic field due to the movement of reduced fluxion [38, 39].

In this study, the tail side of resistivity curves is shifted to lower temperature with the increase in magnetic field. T_c values of prepared samples based on these results show that T_c values are decreased with the increase in magnetic field

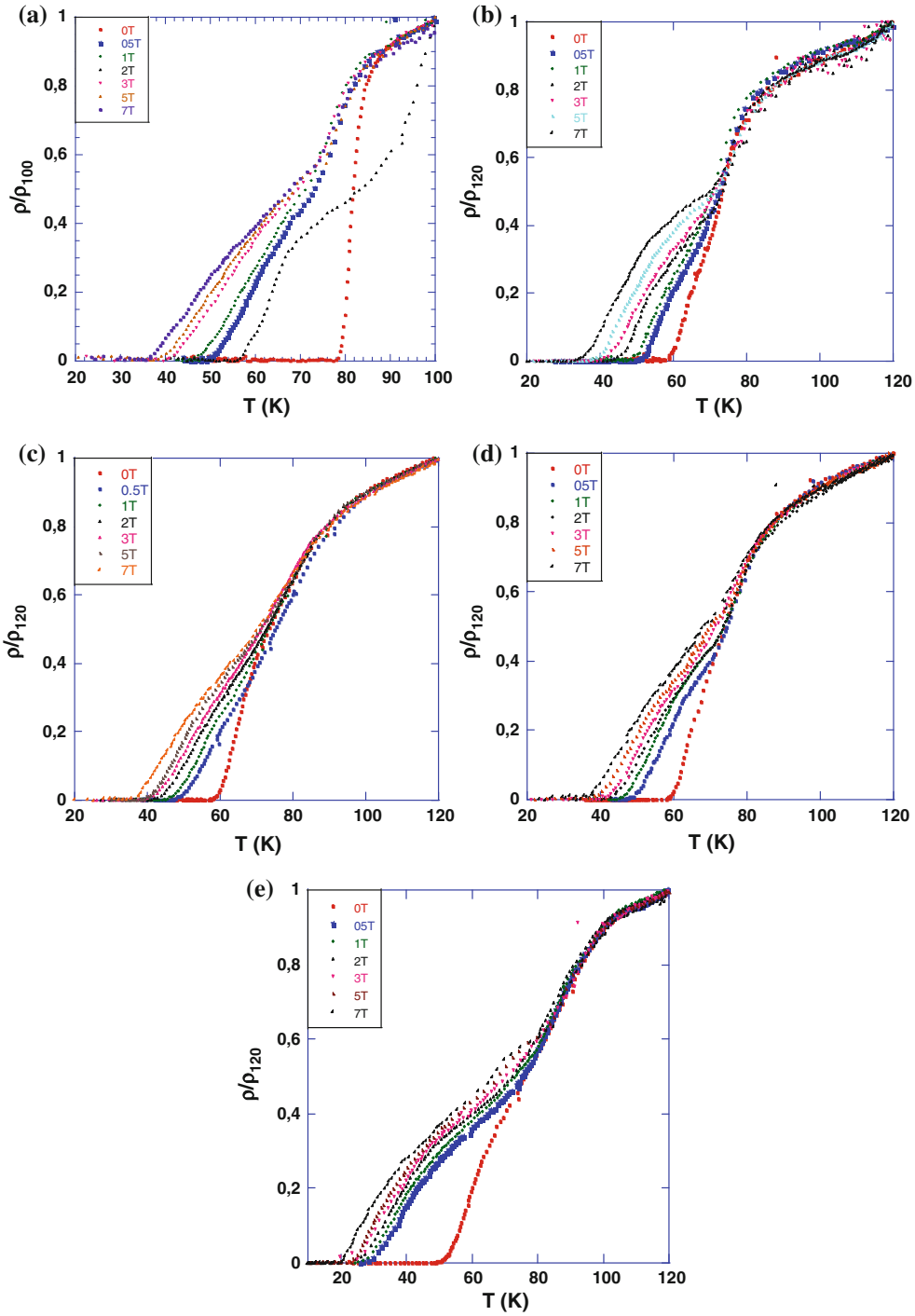

Fig. 6 Normalized resistivity as a function of temperature curves for **a** *M0*, **b** *M1*, **c** *M2*, **d** *M3* and **e** *M4* samples under the various magnetic field

and the addition. This decrease can be explained by the help of weak links between the superconducting grains [40].

3.8 Activation energy calculation

Reaction occurs through the exchange of valence electrons in chemical bonding. For this reason, valence electrons of two atoms need to interact with each other for a reaction to occur. This interaction is possible with an energy which makes collision possible occurring with two atoms beating the thrust force between electrons. The small amount of energy adequate for activation is called as activation energy and it is presented with U_0. The relationship between conductivity and activation energy is supplied with Eq. (1).

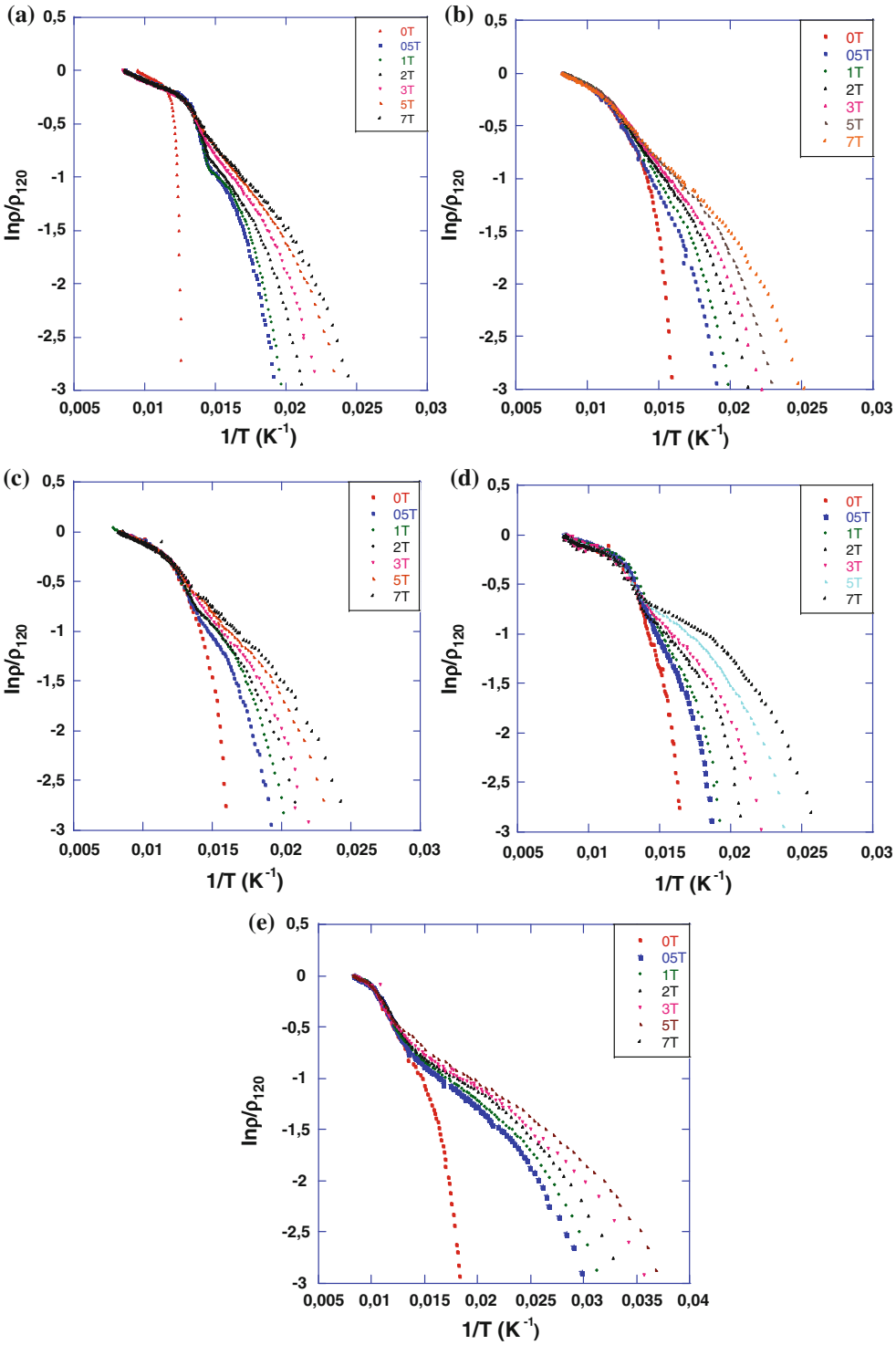

Fig. 7 In ρ/ρ_o versus 1/T graphs of the samples

The activation energy of the samples is found for a part of the transition resistivity at low temperatures to be fitted as linear. Logarithmic resistivity values as a function of the inverse of temperature are drawn under different applied magnetic fields in Fig. 7. Also the activation energy is computed.

The calculated activation energies are provided in Table 4. According to these results, it can be said that activation energy increased to *M3* sample with Nd_2O_3 addition and decrease with increasing magnetic field.

Activation energy decreased significantly with increasing magnetic field. In addition, all the samples showed similar characteristic curves. U_o decreased significantly till 1 T decreased very less in higher magnetic field values. Because the field applied under 1 T is included only in

Table 4 Activation energy values for the all samples

Samples	Activation energies (J/mol)						
	0 T	0.5 T	1 T	2 T	3 T	5 T	7 T
M0	7,766	4,034	3,648	2,740	2,616	1,995	1,830
M1	5,945	3,966	3,478	3,145	2,880	2,620	1,630
M2	5,404	3,860	3,408	2,582	2,081	1,848	1,546
M3	5,313	3,663	3,279	2,367	1,983	1,835	1,504
M4	2,519	1,340	1,247	828	847	817	550

intergranular region. The samples prepared, showed different energy values under the same magnetic field values. This issue is caused by the presence of varied superconductivity levels of samples between the grains [41, 42].

According to this result, the commitment of activation energy to applied field and Nd_2O_3 addition can be associated with porosity, grain misorientation and weak connections between layers in the structure.

4 Conclusions

In this study the role of Nd_2O_3 addition on the superconducting and structural properties of *Bi-2212* superconducting samples, prepared by the solid-state reaction method, has been analyzed. *XRD*, *SEM* and *EDS* measurements for the structural analyses, electrical resistivity measurements (ρ-T) with and without magnetic field for superconducting properties have been carried out. In addition to this, the activation energy of all samples has been calculated using resistivity measurements. According to these results:

- According to *XRD* analyses, *c* parameter of the samples decreased with the increase of Nd_2O_3 doping. However, in *a* parameter, there is a systematical increase with increasing Nd_2O_3 doping. Also, when we analyze the volume fractions according to the change of dope amount, it has been found that *Bi-2212* phase rate decreases with doping (Table 1). No other detectable phases are obtained which show that the majority of *Nd* ions settle into the crystal structure. This result shows that the majority of *Nd* ions enters into the *Bi-2212* crystal structure.
- When the *SEM* images were analyzed, it has been observed that the grains get smaller and a little melting occurs. The results of grain size, calculated using *XRD* peaks, support our *SEM* interpretations.
- When it is compared with other elements, there is a crucial decrease in the percentage of *Sr* concentration in all samples with the increase of Nd_2O_3 addition. As a result, Nd^{+3} ions might enter into the crystal structure by replacing with Sr^{+2} ions.
- As can be seen in Table 3, the hole carrier concentration decreases from 0.105 to 0.089 with decreasing T_c and increasing *Nd* concentration. Also, because of the holes are very important for superconductors, the decreasing holes leads to defects in superconductivity.
- In the electrical resistivity measurements, the temperatures at which *M0*, *M1*, *M2*, *M3* and *M4* samples show zero resistivity are found as in the order of 79, 59, 59, 58 and 50 K. When the dope increases, carrier concentration also decreases; therefore, the decrease in T_c can be caused by the decrease of the charge carriers.
- Using R-T measurements, we can say that the activation energies calculated with Arrhenius equation have increased with Nd_2O_3 doping till *M3* and have decreased with the increase of magnetic field.

References

1. K.H. Müller, A.J. Pauza, Physica C **161**, 319 (1989)
2. N. Ghazanfari, A. Kilic, A. Gencer, H. Ozkan, Solid State Commun. **144**, 210 (2007)
3. T. Makise, S. Uchida, S. Horii, J. Shimoyama, K. Kishio, Physica C **460**, 772 (2007)
4. G. Yildirim, Y. Zalaoglu, M. Akdogan, S.P. Altintas, A. Varilci, C. Terzioglu, J. Supercond. Nov. Magn. **24**, 2153 (2011)
5. H. Maeda, Y. Taraka, M. Fukutomi, T. Asano, J. Appl. Phys. **27**, L209 (1988)
6. O. Ozturk, M. Akdogan, C. Terzioglu, A. Gencer, J. Phys: Conf. Ser. **153**, 012024 (2009)
7. L. Pierre, J. Schneck, D. Morin, J.C. Toledona, J. Primot, C. Daguet, H. Savary, J. Appl. Phys. **68**, 2296 (1990)
8. R.K. Nkum, W.R. Datars, Physica C **190**, 465 (1992)
9. K.K. Nanda, M. Muralidhar, V.B. Hari, Physica C **204**, 299 (1993)
10. S. Kambe, Y.C. Guo, S.X. Dou, H.K. Liu, Y. Wakahara, H. Maeda, K. Kakimoto, M. Yavuz, Supercond. Sci. Technol. **11**, 1061 (1998)
11. C. Terzioglu, M. Yilmazlar, O. Ozturk, E. Yanmaz, Physica C **423**, 119 (2005)
12. V.G. Prabitha, A. Biju, R.G. AbhilashKumar, P.M. Sarun, R.P. Aloysius, U. Syamaprasad, Physica C **433**, 28 (2005)
13. M. Dogruer, Y. Zalaoglu, A. Varilci, C. Terzioglu, G. Yildirim, O. Ozturk, J. Supercond. Nov. Magn. **25**, 961–968 (2012)
14. T. Mito, A. Sagara, S. Imagawa, S. Yamada, K. Takahata, N. Yanagi, H. Chikaraishi, R. Maekawa, A. Iwamoto, S. Hamaguch, M. Sato, N. Noda, K. Yamauchi, A. Komori, O. Motojima, Fusion Eng. Des. **81**, 2389 (2006)
15. J. Zsako, J. Phys. Chem. **72**, 2406–2411 (1968)
16. G. Yildirim, M. Dogruer, O. Ozturk, A. Varilci, C. Terzioglu, Y. Zaloglu, J. Supercond. Nov. Magn. **25**, 893–903 (2012)
17. M. Erdem, O. Ozturk, E. Yucel, S.P. Altintas, A. Varilci, C. Terzioglu, I. Belenli, Phys. B **406**, 705–709 (2011)
18. U. Marvin Herrera, V. Roland Sarmago, Ceram. Int. **30**, 1611–1614 (2004)
19. S. Altin, M.A. Aksan, M.E. Yakinci, Solid State Sci. **13**, 879–886 (2011)
20. I. Karaca, S. Celebi, A. Varilci, A.I. Malik, Supercond. Sci. Technol. **16**, 100 (2003)
21. V. Mihalache, G. Aldica, J. Optoelectron. Adv. M. **9**, 919–922 (2007)

22. M. Okada, Supercond. Sci. Technol. **13**, 29 (2000)
23. D. Yegen, A. Varilci, M. Yılmazlar, C. Terzioglu, I. Belenli, Physica C **466**, 5–10 (2007)
24. O. Ozturk, E. Asikuzun, G. Yildirim, J. Mater. Sci. Mater. Elect. **24**, 1274–1281 (2013)
25. M. Runde, IEEE T. Appl. Supercond. **5**, 813 (1995)
26. A. Godeke, D. Cheng, D.R. Dietderich, C.D. English, H. Felice, C.R. Hannaford, S.O. Prestemon, G. Sabbi, R.M. Scanlan, Y. Hikichi, J. Nishioka, T. Hasegawa, IEEE T. Appl. Supercond. **18**, 516 (2008)
27. L. Shi, Y. Gu, L. Chen, Z. Yang, J. Ma, Y. Qitan, Mater. Lett. **58**, 3301–3303 (2004)
28. J. Jiang, Mater. Lett. **61**, 3239–3242 (2007)
29. O. Ozturk, E. Asikuzun, M. Erdem, G. Yildirim, O. Yildiz, C. Terzioglu, J. Mater. Sci. Mater. Elect. **23**, 511–519 (2012)
30. J. Torrens-Serra, I. Peral, J. Rodriguez-Viejo, M.T. Clavaguera-Mora, J. Non-Cryst. Solids **358**, 107–113 (2012)
31. O. Ozturk, E. Asikuzun, S. Kaya, M. Coskunyurek, G. Yildirim, M. Yilmazlar, C. Terzioglu, J. Supercond. Nov. Magn. **25**, 2481–2487 (2012)
32. A. Biju, P.M. Sarun, R.P. Aloysius, U. Syamaprasad, J. Alloy. Compd. **454**, 46–51 (2008)
33. M.F. Azzouz, A. Mchirgui, B. Yangui, C. Boulesteix, B.M. Salem, Physica C **356**, 83–86 (2001)
34. K. Kocabas, S. Sakiroglu, M. Ciftcioglu, I. Ercan, H. Epik, O. Bilgili, J. Supercond. Nov. Magn. **22**, 749–754 (2009)
35. M.R. Persland, J.L. Tallon, R.G. Buckley, R.S. Liu, N.E. Floer, Physica C **176**, 95–105 (1991)
36. T. Kucukomeroglu, E. Bacaksiz, C. Terzioglu, A. Varilci, Thin Solid Films **516**, 2913–2916 (2008)
37. D. Yazici, M. Erdem, B. Ozcelik, J. Supercond. Nov. Magn. **25**, 1811–1816 (2012)
38. G.L. Bhalla, A. Malik Pratima, K.K. Singh, Physica C **391**, 17–24 (2003)
39. J.S. Moodera, R. Meservey, J.E. Tkaczyk, C.X. Hao, G.A. Gibson, P.M. Tedrow, Phys. Rev. B **37**, 619–622 (1988)
40. N.P. Liyanawaduge, A. Kumar, S. Kumar, B.S.B. Karunarathne, V.P.S. Awana, J. Supercond. Nov. Magn. **25**, 31–37 (2012)
41. E. Govea-Alcaide, I. Garcia-Fornaris, P. Mune, R.F. Jardim, Eur. Phys. J. B **58**, 373–378 (2007)
42. J. Albrecht, C.H. Jooss, R. Warthmann, A. Forkl, H. Kronmüller, Phys. Rev. B **57**, 10332–10335 (1998)